Development of three-dimensional optimization of a small-scale radial turbine for solar powered Brayton cycle application

Daabo, Ahmed M.; Al Jubori, Ayad; Mahmoud, Saad; Al-dadah, Raya K.

DOI:
10.1016/j.applthermaleng.2016.09.147

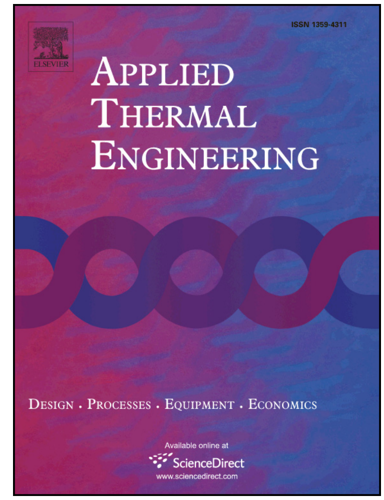

Research Paper

Development of Three-dimensional Optimization of a Small-scale Radial Turbine for Solar Powered Brayton Cycle Application

Ahmed M. Daabo, Ayad Al Jubori, Saad Mahmoud, Raya K. Al-Dadah

PII: S1359-4311(16)31923-8
DOI: http://dx.doi.org/10.1016/j.applthermaleng.2016.09.147
Reference: ATE 9172

To appear in: *Applied Thermal Engineering*

Received Date: 4 July 2016
Revised Date: 30 August 2016
Accepted Date: 25 September 2016

Please cite this article as: A.M. Daabo, A. Al Jubori, S. Mahmoud, R.K. Al-Dadah, Development of Three-dimensional Optimization of a Small-scale Radial Turbine for Solar Powered Brayton Cycle Application, *Applied Thermal Engineering* (2016), doi: http://dx.doi.org/10.1016/j.applthermaleng.2016.09.147

Development of Three-dimensional Optimization of a Small-scale Radial Turbine for Solar Powered Brayton Cycle Application

Ahmed M. Daabo[a, b*], Ayad Al Jubori[a], Saad Mahmoud[a], Raya K. Al-Dadah[a]
[a] The University of Birmingham, School of Engineering,
Edgbaston, Birmingham, B15-2TT, UK
Email: axd434@bham.ac.uk
[b] The University of Mosul, Mech. Eng. Dept. Iraq

Abstract

Numerical simulation was carried out to optimize the design of a small-scale radial turbine. One-dimensional (1D) Mean Line (ML) approach and three-dimensional computational fluid dynamic (3D CFD) simulations, using 3D Reynolds-Averaged Navier-Stokes (RANS) models with the shear stress transport (SST) turbulence model in ANSYS®15- CFX, were employed to achieve the best turbine performance and consequently cycle efficiency. For the current study, a new methodology that integrates the Brayton cycle analysis with modelling of a highly efficient small -scale radial turbine at a wide range of inlet temperatures was developed. A multi-objective function was utilized for optimizing the designed radial turbine power in the range of 1.5 to 7.5 kW. This method has been developed in order to find the optimum design, from an aerodynamic point of view. After applying a well-designed range of parameters for both the stator and the rotor, the results demonstrated an excellent improvement in the turbine efficiency from 82.3% to 89.7% for the same range of output power. Moreover, the effect of the turbine inlet temperature, rotational speed and pressure ratio was further studied and presented in this paper. Finally, the overall cycle efficiency showed an excellent improvement of about 6.5% for the current boundary conditions; and it yielded more than 10% with the increase in the inlet temperature and the pressure ratio. Such results highlight the potential and the benefits of the suggested methodology to achieve a high performance (i.e. turbine efficiency and cycle efficiency).

Keywords: Small scale radial turbine, Solar Brayton cycle, CFD analysis, 3D Optimization, Genetic algorithm.

1- Introduction

The demand for energy is continually increasing day after day, but at the same time, investigations around the world into sustainable sources of power are growing in number. Solar energy is considered one of the main renewable energy sources which can play an important role in decreasing CO2 emissions. It can be efficiently used to generate electricity using different types of thermal power cycles, such as the Brayton cycle.

Moreover, small scale turbines are considered as a promising technology because of their low initial costs, low maintenance, durability and simple construction. Furthermore, they can offer a solution for the power generation demand in domestic or even remote areas. In order to increase the cycle efficiency, one of the main effective ways is to improve the turbines' performance.

Much research has been carried out regarding both the solar Brayton cycle thermodynamic analysis and the selection of the appropriate boundary conditions of energy as heat sources such as [1-4]. For example, an attempt to enhance the overall efficiency of the small-scale solar Brayton cycle, by optimizing both the receiver and the parabolic concentrator, has been achieved by Le Roux at al. [5]. Riazi and Ahmed [6] studied the effect of specific heat ratios for three different working fluids and for air, helium and tetrafluoromethane, on the efficiency of small scale solar energy. A regenerative closed Brayton cycle was analysed in terms of the influence of temperature ratio and the minimum to maximum gas temperature. Their results showed that the higher the specific ratio of the analysed fluid, the higher the cycle efficacy. Moreover, they also suggested that for small-scale Brayton cycles, the performance of lower specific ratios is better as this scale only accumulates a small amount of heat. However, the performance of turbines was not included in all the studies mentioned above as on the shelf turbines were used. Two important parameters have to be carefully considered, as they lead to better preliminary design. Both the loading coefficient and the exit flow coefficient contribute in [7]. Intensive analyses in order to enhance the performance of scroll expander were conducted in [8-10]. Mean line analysis for radial turbines for organic Rankin cycle applications was achieved by many researchers [11-16]. However, no more 84% Total-To-Static efficiency for the studied models of radial turbine have been attained [12]. It is clear that the 3D computational fluid dynamics (CFD) leads to more enhancement in the aerodynamic performance. Three-dimensional optimization design work on ORC radial turbines was demonstrated in [17-19]. On the other hand, modelling and optimization of axial turbines was conducted in [20-21]. Sauret [22] carried out intensively numerical work on a high pressure radial turbine. The author started his study from the preliminary design passing through 3D simulation; then the impact of tip clearance as well as the importance of the diffuser on the turbine's performance was examined at wide range of boundary conditions. The author then validated her design against some experimental data from the literature. Regarding the compressed air radial turbine, it can be seen that only some efforts have been made by different researchers who studied the performance of radial turbines with different design factors as well as boundary conditions. With the aim of identifying the possible acoustic sources which occurs, Marsan and Moreau [23] studied the effect of stator wakes and trailing edge on the impeller blades of radial turbine. In their study the authors showed that the interface regime between the stator and rotor causes pressure fluctuations to the flow passes through these surfaces. They emphasized that the tip clearance losses should not be neglected in analytical studies. Together CFD and FE analysis of relatively high pressure ratio and low inlet temperature, 5 bar and 400 K, radial turbine was conducted in [24]. The output power and efficiency of the investigated turbine were 36.4 and 85% respectively. With comparatively accepted deviation, the authors validated their simulation work using an experimental data. For compressed air turbine optimizations, Tsalicoglou1 and Phillipsen [25] used an iterative method that conducted in-house and commercial CFD codes to decrease the amount of working fluid mass flow rate. This results in changing the turbine blade geometry modifications with some improvement in efficiency. However, with the limitation of the allowed number of design parameters' evaluations, multiple runs were required. As a single objective function, particle swarm optimization was used in their study. An integrated optimization of a 100 kW radial turbine was reported by Lei Fu et al [26]. In their study, an enhancement in terms of aerodynamic and structural performance was achieved. However, the optimization carried out on the rotor while the stator was not considered in their study. Also, each part of optimization was completed separately in two different codes and that might be the reason for the relatively low maximum efficiency value that has been achieved, 82%. Zhang and Ma [27] used the multi-objective algorithm technique for optimizing only the rotor of a radial turbine. Even though the authors claimed the optimized rotor experienced better performance especially in off-design conditions with about an 8% increment in its efficiency, the maximum value that the turbine reached was also low, about 77%.

An intensive study on the relation between optimization of computational time and the chosen range of the database, as well as the selection of the suitable optimization method was reported in [28]. In his study the author emphasized that selecting the closer setting to the optimum parameters not only results in further improvements of the convergence, but also contributes to better rotor geometry performance. Three-dimensional multi-objective optimization for a turbocharger radial turbine impeller designed for automotive applications was applied in [29]. With the aim of maximizing its total-to-static efficiency and the impeller moment of inertia, and at the same time keeping mechanical stresses below a maximum allowable value, the maximum value of efficiency reached was only 80%.

To the best of the authors' knowledge no work has been published on the 3D multi-objective optimization of the two main parts of radial turbines: the stator and rotor, together especially for this scale of turbines. So, this paper tries to focus on design; such as turbine design which creates as high as possible efficiency and output power to the cycle but with keeping both the rotational speed and the mass flow rate at their minimum values.

2- Methodology

In this study the computational fluid dynamic CFD techniques, using ANSYS®15 VISTA, was utilised in order to first initiate a Mean Line (ML) design for the Small Scale Radial Turbine SSRT with relatively sufficient performance. Then, 3-D model was improved using ANSYS®15 CFX tool, which precisely figure out the aerodynamic flow behaviour, analyse were followed in order to have more accurate and better outcomes for the SSRT. After the best design shape for both the stator and rotor was achieved, a number of the most influences parameters were determined and chosen with the aim of optimizing the full blades shape of the SSRT using the 3D Design Exploration feature of ANSYS®15 which employed the genetic algorithm for the multi-objective optimization. Moreover, the results have been directly integrated with the Brayton cycle code which was initiated using the Engineering Equation Solver (EES) software [30].

3- Thermodynamic Analysis of Brayton Cycle

The traditional thermal Brayton cycle consists of the compressor, the combustion chamber, the turbine to extract the air's potential energy and transfer it to mechanical energy; and a pre-heater to exploit the exhaust energy, which will be otherwise lost to the environment and also to preheat the cold air before entering the source of heat. However, the solar powered Brayton cycle shown schematically in Fig. 1, consists of a compressor (1-2), thermal receiver (3-4) and a turbine (4-5). A recuperator, (2- 3), is used to recover heat from the turbine exit's hot air. The current study aimed to be fitted with the application of small scale solar powered Brayton cycle which of course its efficiency can be enhanced by improving the efficiency of its component. The compressor power is given by [5]:

$$\mathrm{W_C} = \frac{Cp\, T_1 (\mathrm{R}_C \mathrm{K} - 1)}{\eta_\mathrm{C}} \tag{1}$$

Where the compressor pressure ratio equals $R_c = P_2 / P_1$ and in contrast the turbine pressure ratio is: $R_t = P_4 / P_5$

The amount of heat supply by the solar receiver per unit mass of working fluid flow is:

$$Q_\mathrm{Net} = (\mathrm{T}_4 - \mathrm{T}_3) \tag{2}$$

The heated working fluid exits from the solar receiver and passes through the turbine to generate power; the power output from the turbine is given by:

$$\mathrm{W_T} = Cp\, \eta_\mathrm{T} T_4 (1 - \mathrm{R}_T - \mathrm{K}) \tag{3}$$

If the pressure loss coefficient is defined to be X, the above formula can be written as:

$$W_T = Cp\,\eta_T T_4(1 - (XR_c) - K) \quad (4)$$

The exhaust's working fluid exits from the turbine to the atmosphere and on its way it will pass through the recuperator. The heat gained by incoming compressed air and the heat rejected through the leaving air is given by the next two equations respectively:

$$Q_c = \dot{m}(h_2 - h_3) \quad (5)$$

$$Q_{cRej} = \dot{m}(h_5 - h_2) \quad (6)$$

The extent to which a recuperator approaches an ideal recuperator is called the effectiveness, ε, and is defined as:

$$\varepsilon = \frac{H_3 - H_2}{H - H_2} \quad (7)$$

The net power output from the cycle is given by:

$$W_{net} = W_t - W_C \quad (8)$$

This can also be written as:

$$W_{net} = Cp\left[\eta_T T_4(1 - (XR_c) - K) - \frac{T_1(R_C K - 1)}{\eta_C}\right] \quad (9)$$

The thermal Brayton cycle efficiency is given by:

$$\eta_{th} = \frac{W_{net}}{Q_{Net}} \quad (10)$$

The above equation can be formulated in terms of temperatures and defined as the following:

$$\eta_{th} = \frac{\eta_t T_4\left(1 - {(XR_c)}^{-K}\right) - T_1\left(\frac{R_c^{K-1}}{\eta_c}\right)}{T_4\left(1 - \varepsilon\left\{1 - \eta_t\left(1 - {(XR_c)}^{-K}\right)\right\}\right) - T_1(1 - \varepsilon)\left(1 + \left(\frac{R_c^{K-1}}{\eta_c}\right)\right)} \quad (11)$$

As it is shown in Fig. 1 the cycle consists of different components and each one of these component needs to be carefully designed. The selection of the best design parameters of the turbine will lead to higher turbine isentropic efficiency, power output. This certainly will enhance the overall efficiency of the cycle and the system performance. Fig. 2 illustrates their T-S (temperature-entropy) diagram.

4- Mean Line Design of Radial Turbine [12, 31-41]:

The initial shape blade as well as its dimensions such as nominal hub and shroud diameters, the blade number and thickness, the trailing and leading edges can be determined using the ML design [41]. Together Figs. 3 &4 show the velocity triangles and their relative thermodynamic processes. The two dimensionless parameters that have been used in the ML design of radial turbine are the loading (ψ) and flow (ϕ) coefficients. These two parameters are together used to determine the exact velocity triangle shapes and then calculate turbine efficiency through the stage as shown in equations 12-14.

$$\Psi = \frac{\Delta h_{actual}}{{U_4}^2} \tag{12}$$

$$\emptyset = \frac{C_{m5}}{U_4} \tag{13}$$

$$\Delta h_{actual} = \Delta h_{isentropic} \eta_{turbine,stage,ts} \tag{14}$$

The relations that connect hub and tip diameter in radial turbine as well as the rotor number of vanes are:

$$r_{5_t} = \sqrt{\frac{A_5}{\pi} + r_{5hub}^2} \tag{15}$$

$$Z_{rotor} = \frac{\pi}{30}\,(\,110 - \,\alpha_2)\tan(\alpha_2) \tag{16}$$

The losses in enthalpy due to the tip clearance are consisting of both the axial and radial clearance. So, these clearances as well as the secondary losses are calculated by the next few equations 17- 23,

$$\Delta h_{tip,clearnace} = \frac{U_3^4\, Z_{rotor}}{8\pi}\left(0.4\,\varepsilon_x C_x + 0.75\,\varepsilon_r\, C_r - 0.3\,\sqrt{\varepsilon_x \varepsilon_r C_x C_r}\right) \tag{17}$$

$$C_x = \frac{1 - \left(\frac{r_{5tip}}{r_4}\right)}{C_{m4}\, b_4} \tag{18}$$

$$C_r = \left(\frac{r_{5tip}}{r_4}\right)\frac{l_{rotorx} - b_4}{C_{m5}\, r_5 b_5} \tag{19}$$

$$l_{rotorx} = 1.5\left(r_{5tip} - r_{5hub}\right) \tag{20}$$

$$\varepsilon_x = \varepsilon_r = 0.04\left(r_{5tip} - r_{5hub}\right) \tag{21}$$

$$\Delta h_{secondary} = \frac{C_4^2\, d_4}{Z_{rotor}\, r_c} \tag{22}$$

$$C_x = \left[\overline{Re}\left(\frac{d_4}{2\, r_c}\right)^2\right]^{0.05}\left[\frac{W_4 + \left(\frac{W_{5tip} + W_{5hub}}{2}\right)}{2}\right]^2 \frac{l_{hyd}}{h_{hyd}} \tag{23}$$

The exit kinetic loss can be computed using the following equation,

$$\Delta h_{exit} = 0.5 C_5^2 \tag{24}$$

In nozzle and volute, on the other hand, after obtaining the friction factor f from moody chart, the differences in the enthalpy because of the friction effect, and Reynolds number can be determined by the next two equations:

$$\Delta h_{friction,nozzle} = 4 f_{nozzle} \bar{C}^2\, \frac{l_{hyd,nozzle}}{d_{hyd,nozzle}} \tag{25}$$

$$f = 8\left[\left(\frac{8}{Re}\right)^{12} + \left(\left[2.475\ln\left(\frac{1}{\left(\frac{7}{Re}\right)^{0.9} + 0.27PR}\right)\right]^{16} + \left[\frac{37530}{Re}\right]^{16}\right)^{-1.5}\right]^{\frac{1}{12}} \quad (26)$$

After determining the fluid mass flow rate, its density and absolute velocity, the maximum radius and volute radius can be defined using the equations from 27- 29,

$$A_1 = \frac{\dot{m}_{working\ fluid}}{\rho_1 C_1} \quad (27)$$

$$r_{volute} = \sqrt{\frac{A_1}{(0.75\pi + 1)}} \quad (28)$$

$$d_{max} = 2(\,r_1 + r_{volute}) \quad (29)$$

The losses which are associated with volute geometry and then the total losses in enthalpy and the total to total efficiency are defined in the last three equations:

$$\Delta h_{loss,volute} = \frac{r_{volut}\, C_2^2}{2} \quad (30)$$

$$\Delta h_{loss,total} = \Delta h_{loss,volute} + \Delta h_{friction,nozzle} + \Delta h_{tip,clearance}$$

$$+\Delta h_{secondary} + \Delta h_{frictio} + \Delta h_{exit} \quad (31)$$

$$\left(\eta_{turbine,stage,ts}\right)_{new} = \frac{\Delta h_{actual}}{\Delta h_{actual} + \Delta h_{loss,total}} \quad (32)$$

The designer can easily get the main specifications and thereby the ML deign of turbines. These specifications, in brief, include Inlet boundary conditions such as pressures, temperature, pressure ratio, and output power as well as design parameters like, flow coefficient, loading coefficients, hub to tip radius ratio and number of blade. Finally, estimation the initial estimations of the overall efficiency initial, tip clearance. Fig. 5 illustrates the main steps of the ML design for the SSRT in a flow chart. Table (1) shows the ranges of input factors and boundary of the radial turbine ML design. The results of the 3D base-line BL of the SSRT geometry from the ML design are shown in Table (2).

5- Numerical Analysis of the model

Once the ML design of the SSRT, using the Vista RTD tool, was completed, all the relevant information for building the blade geometry of the rotor was prepared. So, the next step was to export these dimensions in order to create the rotor blade geometry using the Blade-Gen feature in ANSYS CFX. This tool in fact can be used to construct the stator blade as well as the rotor for the studied turbine. The CFX Turbo-Grid was employed in order to generate the required elements for the turbine's fluid domain. The 3D turbulent viscous flow simulation in the whole domain of the SSRT was functioned using the Shear Stress Transport turbulence model with equations of Navier-Stokes.
The assumptions of the 3D CFD simulation are steady state, using a compressible single-phase ideal air gas. Also, the first order upwind advection scheme was selected because it is numerically stable. The SST/k-omega has the ability to treat the low velocity region near the wall through an automatic wall function, to capture the turbulence zone by the specified first node after the wall. The SST/K-

omega model is specifically designed for the complex flow like turbomachinery flow as suggested by [43]. The flow direction was set to be normal to boundary and the average value of y+ was set aside unity as recommended in the CFX-Solver theory guide [43]. The convergence criteria for the residuals of the continuity, energy and the velocity equations were of the order of 10^{-6}. The solutions for all the cases were obtained once the results of the convergence criteria were satisfied.

The CFD simulations were established in order to analysis the SSRT behaviour at both; the nominal and the other off-design conditions. Figure 6A displays the full SSRT as created by the Blade-Gen CFX; while Fig. 6b presents the density of the chosen mesh passage for the rotor blade. The rotor grid number was about 1,200,000 nodes and the stator grid number was around 600,000 using a finer mesh for the adjacent walls of blades. During the optimization procedure 15 parameters have been nominated in order to achieve the required objective function. Those parameters are: the rotor blade number; the rotor blade shape, which is represented by 12 parameters; the stager angle of the stator; and the stator blade number. More details are found in section 6.

6- Validation

Because they have relatively sufficient data, the references [46 & 47] have been chosen and deeply investigated in order to validate the current work. The validation results showed good agreement between the current work and the two chosen ones. While the first validation, which was with reference [46], the CFD technique was used in order to validate the current work, however, in the second validation, with reference [47], only the 1Dimensional approach was used because relatively little information was provided about the 3Dimensional approach. Regarding the mesh sensitivity, it worth to mention that the turbine model had around 1,000,000 nodes for stator and 2,000,000 for the rotor. It is worth noting that in the zone near to the walls and blade's surface, the grid size was refined in order to sustain a good agreement between computational costs and solution accuracy. The grid sensitivity analysis was carried out based on turbine total to static efficiency as shown in Fig. 8 in order to reach the satisfied number of elements for the chosen mesh type.

The schematic view of the radial turbine that used in Ref [47] is presented in Fig. 7.

Furthermore, Figs. 9A and B showed the comparison between the present work and the two mentioned journals respectively.

The authors referred to the secondary losses of the stator, friction losses of the vaneless-space surface, and the mixing trailing edge and wake losses as reasons for the uncertainty of their results. However, the uncertainty of Ref.[45] was because of the difference in the operating conditions of their rig; especially regarding the hot and normal clearances of the rotor, which increases the tip clearance losses.

7- Results of the Base-line Design

Figure 10 compares the CFD results of the base-line design against the ML design analysis at nominal boundary conditions, shown in Table (1). The values of output power and isentropic efficiency were compared for three different cases: inlet temperature, rotational speed and pressure ratio. Specifically, Figs. 10A and10A$^{/}$ show the values of output power and efficiency at different values of turbine inlet temperatures. In this figure the relative over estimation for the ML analysis in terms of both the turbine output power and the efficiency can be noticed. The main reason for this is the inability of the 1D analysis to elicit the exact behaviour of the fluid. Similarly, Figs. 10B, 10B$^{/}$, 10C and 10$^{/}$ represent the turbine output power and efficiency at different values of its rotational speed and pressure ratio respectively. It can be seen that at each specific boundary condition the output power and efficiency of the turbine reached the peak. Furthermore, this figure shows that the maximum difference in efficiency between the PD and CFD results was about 9% for the case of different inlet temperatures and 6.9% in output power for the case of different pressure ratios because the ML design is not able to capture all properties that the real flow behaves.

8- Multi-objective Optimization and Genetic Algorithm

Engineers still need to search for the best design among the available possible designs. Yet, the term 'best' can come with many meanings and what is excellent in some terms or applications may not be the best in other applications; thereby this term does not have an absolute meaning. Therefore, understanding the optimization procedure in depth will certainly lay the groundwork for optimization of the turbines; especially the Small Scale Turbines (S.S.T.) whose sizes might add to the challenge of their optimization. The term fitness in nature can be represented, from the engineering point of view, as the most robust design. From this point the idea of initiating an Optimized Small Scale Radial Turbine (O.S.S.R.T.) began and is presented in this paper. The operation of the GA starts with a population of random strings and the design variables are represented by these strings. Thereafter, each single string will be assessed to discover the fitness value. Three main well-known operators – reproduction, cross over, and mutation will be run to create a new population of points and then drive the population. The new population will be further assessed and tested in order to terminate the process. However, if the termination criterion is not met, the population will iteratively run using the three mentioned operators and again be evaluated. This procedure will be continued until the termination criterion is reached. The structure of the algorithm is shown in Fig. 11. In this study the objectives include the efficiency, the power output of the turbine, the mass flow rate of the working fluid and the rotational speed. On the other hand, some constraints such as the stator throat area (to deliver the required mass flow rate of air to the rotor), the tip clearance and blade thickness (for manufactural purposes), are also provided.

In this study the multi-objective function was harnessed with the aim of optimizing the designed radial turbine.

Comparing it to single objective optimization, the multi-objective has the ability to maximize or minimize many functions, depending on their constraints, simultaneously.

Differences between the Genetic Algorithm (GA) methods and other traditional optimization methods:

1- Genetic algorithms (GA) work with the coding of the parameter set, not the parameters themselves.
2- GAs search for a population of points, not a single point.
3- GAs use the objective function information and not the derivative or second derivative.
4- GAs use stochastic transition rules, not deterministic rules.

8.1- Aerodynamic Optimization of SSRT

The design exploration package, which is linked in the CFD analysis, is based on the quadratic Response Surface Method (RSM). This method is one of three popular techniques (Kriging, Radial Basis Functions and polynomial Response Surface Model) in surrogate models. This method, which has the best compromise between the computational expense and modelling accuracy, is provided with a polynomial model. In this study, parameterization of the blade geometry and generation of the design points, using the Design of Experiments (DoE) and design of exploration package in ANSYS®15 was carried out. As the multi-objective optimization enables user to choose more than one objective, each; power output and total efficiency of the turbine together with mass flow rate and rotational speed were chosen as objective functions. Then, the response surface approximation (RSA)

[41], which is a statistical functions that connects the output parameters in terms of input parameters (blade profile), will be employed using ANSYS®15. The GA is employed for global exploration. After completing the numerical solution for each single design point, the discrete response for each of them was obtained. The second order polynomial response can be formulated [44, 45] as:

$$f(x) = \beta_0 + \sum_{j=1}^{N} \beta_j x_j + \sum_{j=1}^{N} \beta_{jj} x_j^2 + \sum \sum_{i \neq j}^{N} \beta_{ij} x_i x_j \quad (33)$$

Here, f(x) is the function to be optimized; β characterizes regression coefficients; and x point to a set of the design parameters. However, in a constrained minimization problem, the objective function is replaced by the penalized function which is as follows:

$$P(x) = f(x) + \sum_{j=1}^{N} u_j \langle g(x_j) \rangle^2 + \nu_k \sum_{k=1}^{K} [h_k(x)]^2 \quad (34)$$

Where u_j and ν_k are penalty coefficients, which are usually kept constant throughout the GA simulation. The inequality constraints and equality constraints are g(x) and h(x) respectively. However the fitness function, in terms of a penalized function is as follows:

$$F(x) = \frac{1}{\left(1 + P(x)\right)} \quad (35)$$

If the RSA function is intensively in variation with the design parameters, this leads to redesigning the space sample between the design points and a rebuilt objective function [43]. The main target of the current 3D optimization is to enhance the blade geometry in order to minimize the losses through the passage, in terms of entropy generation; maximize the SSRT efficiency, as well as minimize both the mass flow rate of the working fluid and the rotor rotational speed. Fig. 12 explains the procedure followed during the 3D CFD optimization.

Both parameterization of the blade geometry and choosing the correct range of the parameters are considered very important and critical steps in a successful optimization procedure. Therefore, they need to be carefully selected in order to achieve the requested goal of optimization. Both; the rotor and the stator blade geometries were conducted in the 3D CFD optimization. Unlike the axial rotor blade (the airfoil), the rotor blade geometry is presented via a camber line and layered surface because of its high curvature and the difficulty in representing the exact blade shape using two or three points. As a result, besides the rotor blade number, twelve other parameters, (some of them in terms of the X and Y coordinates), which together represent the rotor blade shape and required throat width, have been selected as input parameters. By doing so, the full definition of the rotor blade will be figured out. Regarding the stator geometry, there are only two parameters which have been chosen. The first is the stagger angle which has a direct impact on the stator shape. The second parameter was chosen to be a constraint objective in order to deliver the same constant mass flow rate to the rotor during the optimization process.

In order to successfully achieve the optimum design for the SSRT, the optimization process was implemented for the range of design boundary conditions shown in Table (1). The blade shape parameterization is one of the fundamental aspects of a reliable optimization procedure, as it requires generating wide ranges of acceptable blade geometry within groups of design variables and their ranges. The parameterization of the blade's geometry was mainly accomplished for the rotor and only the stator's stagger angle was included. In addition, the stator's blade number (for constrained mass flow rate) was defined as a constraint function. Moreover, three different objectives were nominated as objective functions. Maximizing both the output power and the turbine efficiency were two of the three selected; and minimizing the rotor rotational speed was also desired as the third objective function in the MOGA.

8.2- Results of Optimization

After defining the parameters, the constraints and the objective functions, more than 1200 different design points (proposed solutions) have been initiated depending on random distributed data. The solution took more than 504 continuous hours on the Core I7 3.7 GHz processor and 48 GB RAM Computer. Figs. 13 A, B and C show an example of some proposed solutions as candidate design points. Due to the large number of them, the design points have been separated into three Figs., (A) to (C). Each one has about 250 proposed solutions (which together represent only about 63% of all the design points) in terms of the output power and the turbine efficiency. From the mentioned figures one can see that some candidate points have about 92% turbine efficiency and even higher efficiency than the chosen optimum point. However, because they didn't satisfy the minimum rotational speed objective, these design points have been omitted. Another important issue that can be concluded from these figures is that not all the candidate points can deliver satisfactory results and come up with a solution. It can be seen that some of them are unable to do so. Table (5) presents the optimum and the base-line values of design variables of turbine, while Fig. 14 displays the two shapes of blade; for the base-line and the design.

Figure 15 compares the CFD results of the base-line (CFD- Base) design against the Optimum Point (OP) analysis at nominal and off design boundary conditions. The values of the output power and isentropic efficiency were compared for: inlet temperature, rotational speed and pressure ratio. Specifically, Figs. 15A & 15A$^{/}$ show the values of output power and efficiency at different values of turbine inlet temperature. In this figure the effect of the turbine inlet temperature (fixing all other BCs) is highlighted. While there is a positive relationship between the turbine output power and the inlet temperature, the efficiency reached its maximum point at 450K, as it was the designed point. Similarly, Figs. 15B & 15B$^{/}$ and 15C & 15C$^{/}$ represent the turbine output power and efficiency at different values of its rotational speed and pressure ratio respectively. Furthermore, this figure shows that the turbine efficiency and power output increased with a maximum improvement of about 9.35% in turbine efficiency and 41.08% in power output. The main reason behind this enhancement relates to the amount of losses (such as shock losses, secondary losses and incidence losses) that are largely decreased when the blade shape reached its optimum configuration. Moreover, it is obvious from Fig. 15 that even in the off-design condition the overall performance of the optimized SSRT is by far better than their peers at the BL for the all invistigated boundary conisions. Overall, in its optimum design, the turbine behaves better than the CFD- Base design during the off design conditions especially in terms of the amount of output power.

Fig. 16A demonstrates the loading distribution (represented in terms of pressure distribution) through all the passage of the rotor. The highest velocity of the flow, which is located at the throat area, results in lowest values of pressure on the suction surface. However, the opposite is the case for velocity distribution on the pressure side starting from the leading to the trailing edges. In Fig. 15B, the contours of pressure distribution through all of the turbine passage, stator and rotor, are presented. From this figure it can be seen how the pressure is distributed starting from the highest value in the stator to the lowest at the diffuser.

However, the loss through the rotor passage can be assessed by entropy generation which is an indicator of the amount of aerodynamic losses. From Fig. 17 it is shown that the 3D optimization which is done using the MOGA, was able to decrease the amount of entropy generated within mainly the rotor blade, but also in the stator blade passage, compared to the base-line design and thereby enhance the flow aerodynamically.

9- Results of Brayton Cycle Analysis

Using the Brayton cycle analysis in equations 1-11 to calculate the cycle efficiency for the various boundary conditions, the cycle efficiency at nominal and other boundary conditions, as well as the enhancement that the cycle has achieved is clear in Fig. 18. These improvements are delivered by 3D CFD results and inserted in the cycle modelling as inputs to calculate the overall cycle efficiency.This improvement, which is not constant for all the investigated boundary condtions, is mainly due to the increment that occured in the turbine efficiency. The pressure ratio and inlet temperature values range from 2- 4 and 450 K- 550 K shown in Figs. 18A, B and C respectively. At this point it is worth mentioning that for the nominal conditions, the optimum pressure value that gives maximum cycle efficiency is 3. However, with increasing the turbine inlet temperature the optimum pressure values become 3.5 and 4 at 500 K and 550 K respectively. This is because of the fixed relationship between the turbine inlet temperture and the turbine working pressure ratio. Moreover, for the other boundary conditions of the cycle, with improving the turbine efficiency from about 82% to 89.5 %, the improvement was about 6% at the current nominal condtions, and 5% and 4% at the three investigated temperatures respectively. Finally, it can be seen that the maximum efficiency values which were achieved were about 11%, 18.5% and 27% at the mentioned optimum values of the pressure ratio and for the three inlet tempertures respectively.

10- Conclusions

Numerical simulation was carried out to optimize a small-scale radial turbine with output power in the range of 1.5 to 7.5 kW. A one-dimensional Mean Line approach and three-dimensional CFD simulations, using three-dimensional RANS with the SST turbulence model in ANSYS®15- CFX, were employed to achieve the best turbine performance; and consequently, the highest reachable efficiency for the small-scale solar powered Brayton cycle. This paper demonstrated the following important outcomes:

- The CFD simulation results show good agreement with mean line design results for turbine efficiency and power output.
- A relatively high increment in the isentopic efficiency, from 82.3% to 89.7% for the same range of output power was achieved. This was reached by optimizing the shape and the number of both the stator and the rotor components of the radial turbine.
- The results showed that a small-scale radial turbine can achieve a power output of around 3.5 kW with isentropic efficiency about 89.5% at a relatively low inlet temperature; which can be obtained from solar energy through a parabolic concentrator dish as a heat source.
- It was clear from the 3D CFD optimization results that the MOGA optimizer is considerably beneficial in improving the turbine's performance in terms of both the turbine efficiency and the power output. Consequently, the thermal cycle efficiency has also been increased by about 6% as a result of increasing the turbine's efficiency.
- Also, the blade loading and losses (entropy generation) had significantly improved compared to the base-line design. So, it can be said that the integrated approach between Brayton cycle modelling, PD, 3D CFD simulation and optimization methodologies have potential advantages to achieve a high performance of a small-scale solar powered Brayton system.

The integrated aerodynamic and structural optimization is the next study in order to figure out the mechanical stresses that accompanied the turbine structure during its service.

ACKNOWLEDGMENT

The author thanks the Higher Committee of Developing Education in Iraq HCED for funding this project.

Nomenclature

Symbol	Definition
A	Area (m^2)
b	Axial chord (mm), blade width (mm)
c	Absolute velocity (m/s)
d	Diameter (m)
f	Friction factor (-)
h	Enthalpy (J/kg)
H	Blade height (mm)
i	Incident angle (deg.)
k	Loss Coefficient (-)
l	Length (m)
m	Mass flow rate (kg/s)
p	Pressure (Pa)
PR	Pressure ratio (-)
r	Radius (m)
Re	Reynolds No. (-)
s	Entropy (J/kg. K)
SC	Swirl coefficient (-)
T	Temperature (K)
U	Rotor blade velocity (m/s)
w	Relative velocity (m/s)
W	Power (W)
Z	Blade number in radial turbine (-)
Greek symbols	**Definition**
α	Absolute flow angle (deg.)
β	Relative flow angle (deg.)
ε	Clearance (m)
η	Efficiency (%)
υ	Velocity ratio (-)
ρ	Density (kg/m^3)
φ	Flow coefficient (-)
ψ	Loading coefficient (-)
ω	acentric factor (-)
ζ	Losses (-)
Acronyms	**Definition**
BL	Base-line Design
BCs	Boundary Conditions
CFD	Computational Fluid Dynamics
DoE	Design of Experiment
GA	Genetic Algorithm
LE	Leading edge
ML	Mean Line Design
MOGA	Multi-objective genetic algorithm
ORC	Organic Rankine Cycle
O.S.S.R.T	Optimized Small Scale Radial Turbine
RANS	Reynolds-Averaged Navier-Stockes
RSA	Response Surface Approximation
SST	Shear Stress Transport
TE	Trailing Edge
Subscripts	**Definition**
1-6	Station
m	Meridional direction
r	radial
rel	relative
s	Isentropic
x	Axial

t	Total, stagnation
ts	Total to static
th	Thermal
θ	Tangential/circumferential direction

References

[1] Ordóñez, Juan Carlos, and Adrian Bejan. "Entropy generation minimizations in parallel-plates counter flow heat exchangers." International Journal of Energy Research 24.10 (2000): 843-864.

[2] Le Roux, Willem Gabriel, Tunde Bello-Ochende, and Josua P. Meyer. "Operating conditions of an open and direct solar thermal Brayton cycle with optimised cavity receiver and recuperator." Energy 36.10 (2011): 6027-6036.

[3] Wu, Yuting, et al. "Dynamic simulation of closed Brayton cycle solar thermal power system." ICSETN2004 (2004): 1-6.

[4] Le Roux, Willem Gabriel, Tunde Bello-Ochende, and Josua P. Meyer. "Optimum performance of the small-scale open and direct solar thermal Brayton cycle at various environmental conditions and constraints." Energy46.1 (2012): 42-50..

[5] Le Roux, Willem Gabriel, Tunde Bello-Ochende, and Josua P. Meyer. "The efficiency of an open-cavity tubular solar receiver for a small-scale solar thermal Brayton cycle." Energy Conversion and Management 84 (2014): 457-470.

[6] Riazi, H., and N. A. Ahmed. "Effect of the ratio of specific heats on a small scale solar Brayton cycle." Procedia Engineering 49 (2012): 263-270.

[7] Chen, H., and N. C. Baines. "The aerodynamic loading of radial and mixed-flow turbines." International journal of mechanical sciences 36.1 (1994): 63-79.

[8] Collings, Peter, and Zhibin Yu. "Modelling and analysis of a small-scale Organic Rankine Cycle system with a scroll expander." Proceedings of the world congress on engineering. 2014.

[9] Giuffrida, Antonio. "Modelling the performance of a scroll expander for small organic Rankine cycles when changing the working fluid." Applied Thermal Engineering 70.1 (2014): 1040-1049.

[10] Declaye, Sebastian, Sylvain Quoilin, and Vincent Lemort. "Design and experimental Investigation of a small scale Organic Rankine Cycle using a Scroll Expander." (2010).

[11] Erbaş, Murat, and Atilla Biyikoglu. "Design of low temperature Organic Rankine Cycle and turbine." Power Engineering, Energy and Electrical Drives (POWERENG), 2013 Fourth International Conference on. IEEE, 2013.

[12] Rahbar, Kiyarash, et al. "Modelling and optimization of organic Rankine cycle based on a small-scale radial inflow turbine." Energy conversion and management 91 (2015): 186-198.

[13] Rahbar, Kiyarash, et al. "Parametric analysis and optimization of a small-scale radial turbine for Organic Rankine Cycle." Energy 83 (2015): 696-711..

[14] Han, Sangjo, JongBeom Seo, and Bum-Seog Choi. "Development of a 200 kW ORC radial turbine for waste heat recovery." Journal of Mechanical Science and Technology 28.12 (2014): 5231-5241.

[15] Cho, S., C. Cho, and C. Kim. "A Study of Cycle Analysis and Turbine Design for Obtaining Small-Scaled Power from the Organic Rankine Cycle Using R245fa." (2013).

[16] Fiaschi, Daniele, Giampaolo Manfrida, and Francesco Maraschiello. "Thermo-fluid dynamics preliminary design of turbo-expanders for ORC cycles." Applied energy 97 (2012): 601-608.

[17] Harinck, John, et al. "Performance improvement of a radial organic Rankine cycle turbine by means of automated computational fluid dynamic design."Proceedings of the Institution of Mechanical Engineers, Part A: Journal of Power and Energy 227.6 (2013): 637-645.

[18] Sauret, Emilie, and Yuantong Gu. "Three-dimensional off-design numerical analysis of an organic Rankine cycle radial-inflow turbine." Applied Energy135 (2014): 202-211.

[19] Rahbar K, Mahmoud S, Al-Dadah RK, Moazami N. "One-dimensional and three-dimensional numerical optimization and comparison of single-stage supersonic and dual-stage transonic radial inflow turbines for the ORC, Proceedings of the ASME 2016 Power and Energy Conference, Inpress accepted paper.

[20] Da Lio, L, Manente, G and Lazzaretto, A. New efficiency charts for the optimum design of axial flow turbines for organic Rankine cycles". Energy 2014; 77, pp. 447- 459.

[21] Ennil, Ali Bahr, et al. "Minimization of loss in small scale axial air turbine using CFD modeling and evolutionary algorithm optimization." Applied Thermal Engineering 102 (2016): 841-848.

[22] Sauret, Emilie. "Open design of high pressure ratio radial-inflow turbine for academic validation." ASME Paper No. IMECE2012-88315 (2012).

[23] Moreau, Aurélien Marsan-Stéphane. "ANALYSIS OF THE FLOW STRUCTURE IN A RADIAL TURBINE."

[24] Odabaee, M., Mohsen Modir Shanechi, and K. Hooman. "CFD Simulation and FE Analysis of a High Pressure Ratio Radial Inflow Turbine." 19AFMC: 19th Australasian Fluid Mechanics Conference. Australasian Fluid Mechanics Society, 2014.

[25] Tsalicoglou, Isaak, and Bent Phillipsen. "Design of radial turbine meridional profiles using particle swarm optimization." 2nd International Conference on Engineering Optimization. 2010.

[26] Fu, Lei, et al. "Integrated optimization design for a radial turbine wheel of a 100 kW-class microturbine." Journal of Engineering for Gas Turbines and Power 134.1 (2012): 012301.

[27] Zhang, Qiang, and Chaochen Ma. "Multiple-objective aerodynamic optimization design of a radial air turbine impeller." Remote Sensing, Environment and Transportation Engineering (RSETE), 2011 International Conference on. IEEE, 2011.

[28] Van den Braembussche, R. A. Optimization of radial impeller geometry. VON KARMAN INST FOR FLUID DYNAMICS RHODE-SAINT-GENESE (BELGIUM), 2006.

[29]. Mueller, Lasse, Zuheyr Alsalihi, and Tom Verstraete. "Multidisciplinary optimization of a turbocharger radial turbine." Journal of Turbomachinery135.2 (2013): 021022.

[30] Klein, SA Engineering equation solver. F-chart Software, Middleton, WI; 2013.

[31] Balje, O. "Turbomachines. A guide to Design, Selection and Theory. JohnWiley & Sons." Inc., New York (1981).

[32] Rohlik H. E., "Analytical determination of radial inflow turbine design geometry for maximum efficiency," Tech. Rep. TN D-4384, NASA,Washington, DC, USA, (1968).

[33] Rogers C., "Mainline Performance Prediction for Radial Inflow Turbine in Small High Pressure Ratio Turbine, " VKI Lecture Series 1987-07, (1987).

[34] Whitfield A. and Baines N., "Design of Radial Turbomachines", JohnWiley & Sons, New York, NY, USA, (1990).

[35] Moustapha H., Zeleski M. F., Baines N. C., and D. Japikse, "Axial and Radial Turbines", Concepts NREC, White River Junction, Vt, USA, (2003).

[36] Aungier H., "Turbine Aerodynamics: Axial-Flow and Radial- Flow Turbine Design and Analysis", ASME Press, New York, NY, USA, (2006).

[37] Dixon, S.L. and Hall C., "Fluid mechanics and thermodynamics of turbomachinery". Butterworth-Heinemann, Oxford, UK (2013).

[38] Suhrmann, J.F., Peitsch, D., Gugau, M., Heuer, T., and Tomm, U., 2010, "Validation and development of loss models for small size radial turbines. " Proceedings of ASME Turbo Expo 2010: Power for land, sea and Air GT 2010, Glasgow, UK, Paper No GT (2010)-22666.

[39] Glassman AJ., "Computer program for design and analysis of radial inflow turbines". NASA TN 8164; (1976).

[40] Churchill SW. "Friction-factor equation spans all fluid-flow regimes". Chem Eng (1977);84:91–2.

[41] Wilson, David Gordon, and Theodosios Korakianitis. The design of high-efficiency turbomachinery and gas turbines. MIT press, 2014.

[42] Al Jubori A, Al-Dadah RK, Mahmoud S, Khalil KM, Bahr Ennil AS. "Development of efficient small scale axial turbine for solar driven organic Rankine cycle". Proceedings of ASME Turbo Expo 2016: GT2016, Seoul, South Korea, paper no GT2016-57845.

[43] ANSYS 15 CFX-Solver Theory Guide.

[44] Kim, Jin-Hyuk, et al. "Performance enhancement of axial fan blade through multi-objective optimization techniques." Journal of Mechanical Science and Technology 24.10 (2010): 2059-2066.

[45] Surekha, N., Srinivas Kolla, Deva Raj Ch, and K. Sreekanth. "Optimization of Principal Dimensions of Radial Flow Gas Turbine Rotor Using Genetic Algorithm." Int. J. Scientific& Engineering Research 2012;3:1-6.

[46] McLallin, K.L.; and Haas, J.E., "Experimental Performance and Analysis of 15.04-cm-tip-diameter, Radial-inflow Turbine with Work Factor of 1.126 and Thick Blading". NASA TP-1730, (1980).

[47] Jones, Anthony C. "Design and test of a small, high pressure ratio radial turbine." ASME 1994 International Gas Turbine and Aeroengine Congress and Exposition. American Society of Mechanical Engineers, 1994.

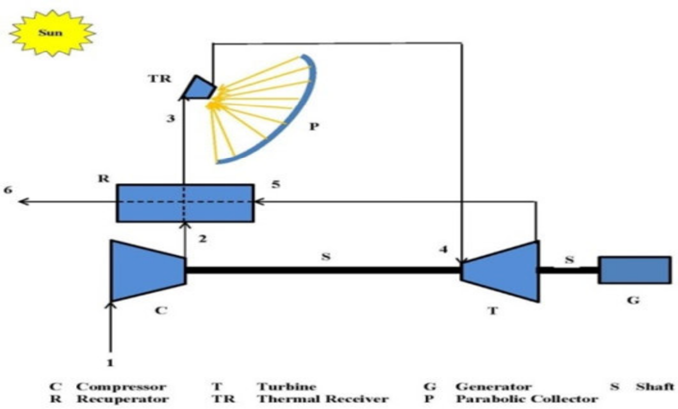

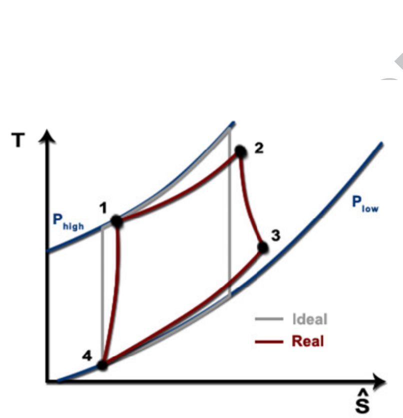

Fig.1. Schematic diagram of CSP-BC system. **Fig. 2.** T-S diagram of Brayton cycle.

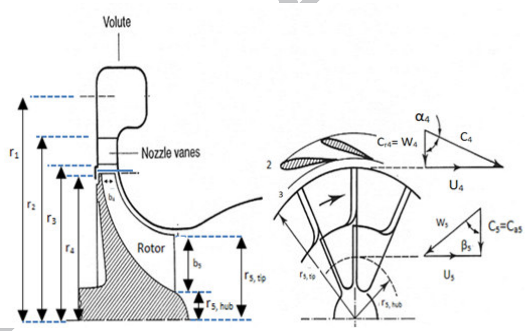

Fig. 3. Schematic view and the meanline velocity triangles of the radial turbine.

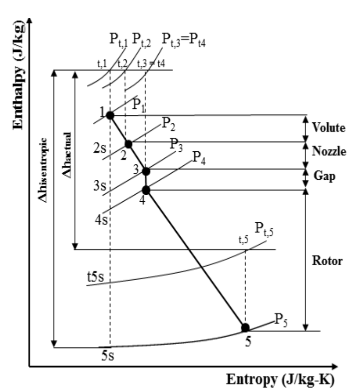

Fig. 4. Enthalpy-entropy diagram of the turbine.

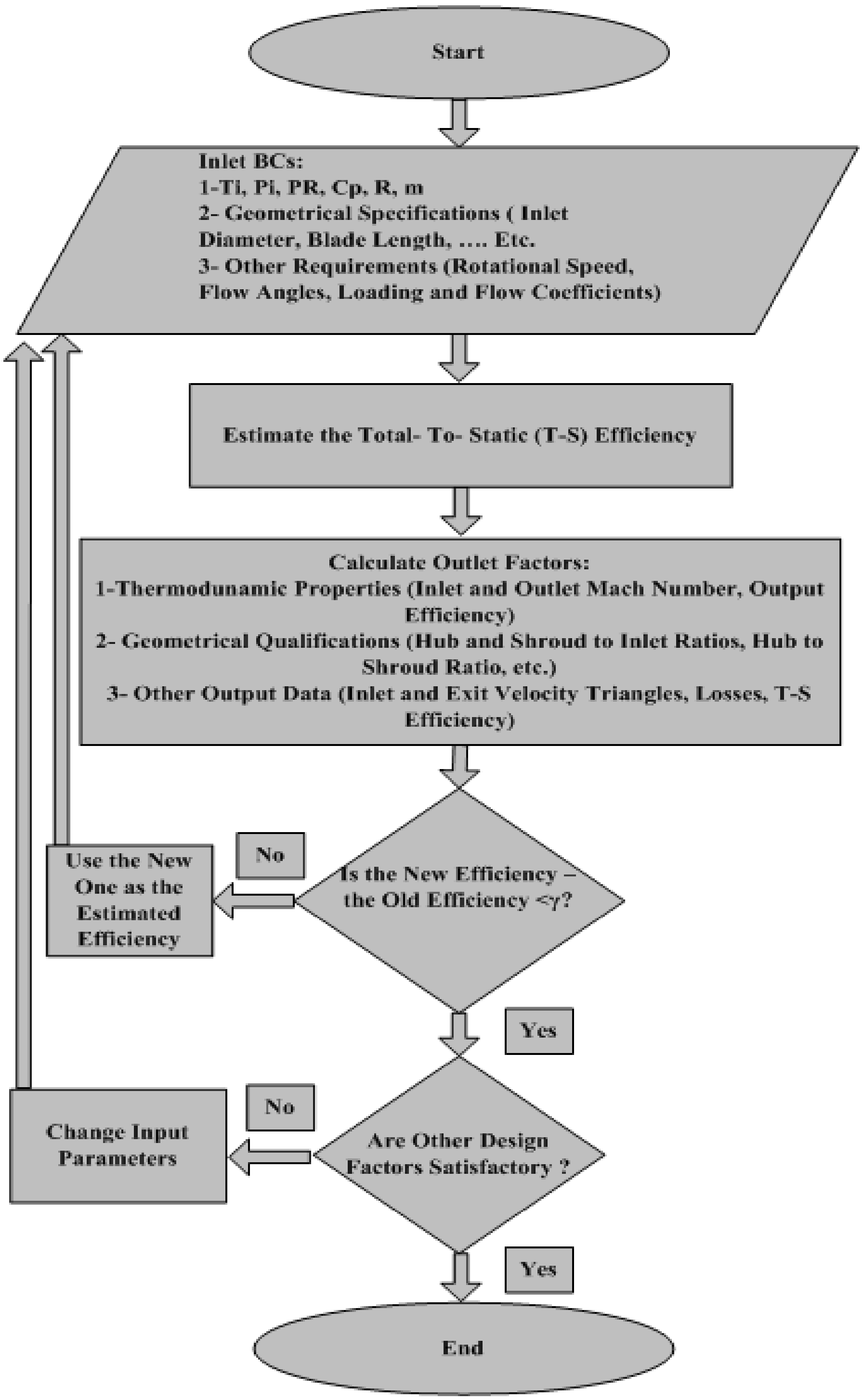

Fig. 5 Algorithm procedure followed for the designed turbines.

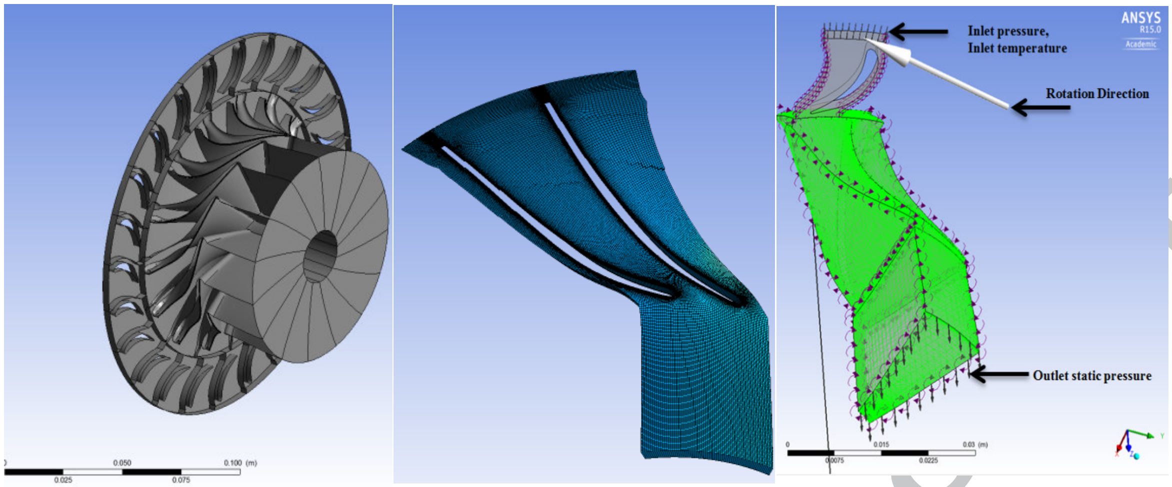

(A) (B) (C)

Fig. 6. Three dimensional view of; (A): Radial turbine geometry, (B): 3D mesh generation for the rotor blade and (C): The coupled stator- rotor domain.

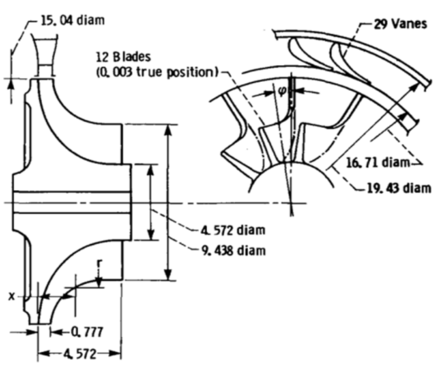

Fig. 7. Schematic view of the radial turbine that used in Ref [47].

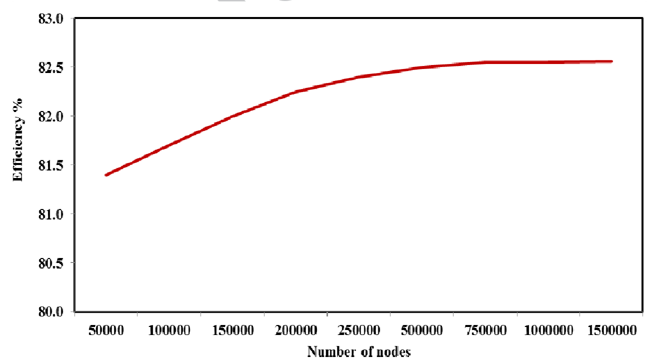

Fig. 8. Mesh sensitivity based on turbine efficiency. Ref [47].

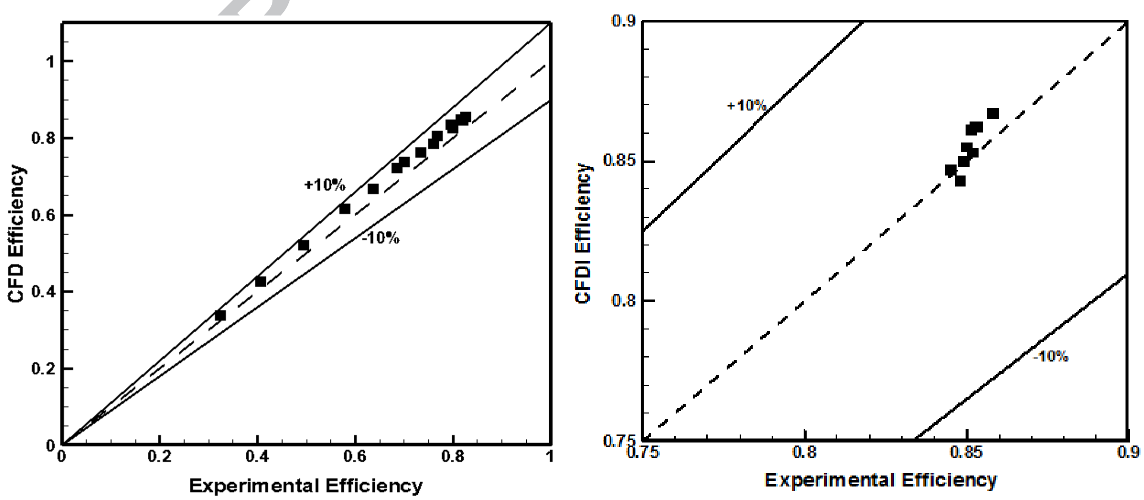

Fig. 9. The efficiency of the current work against two experimental works.

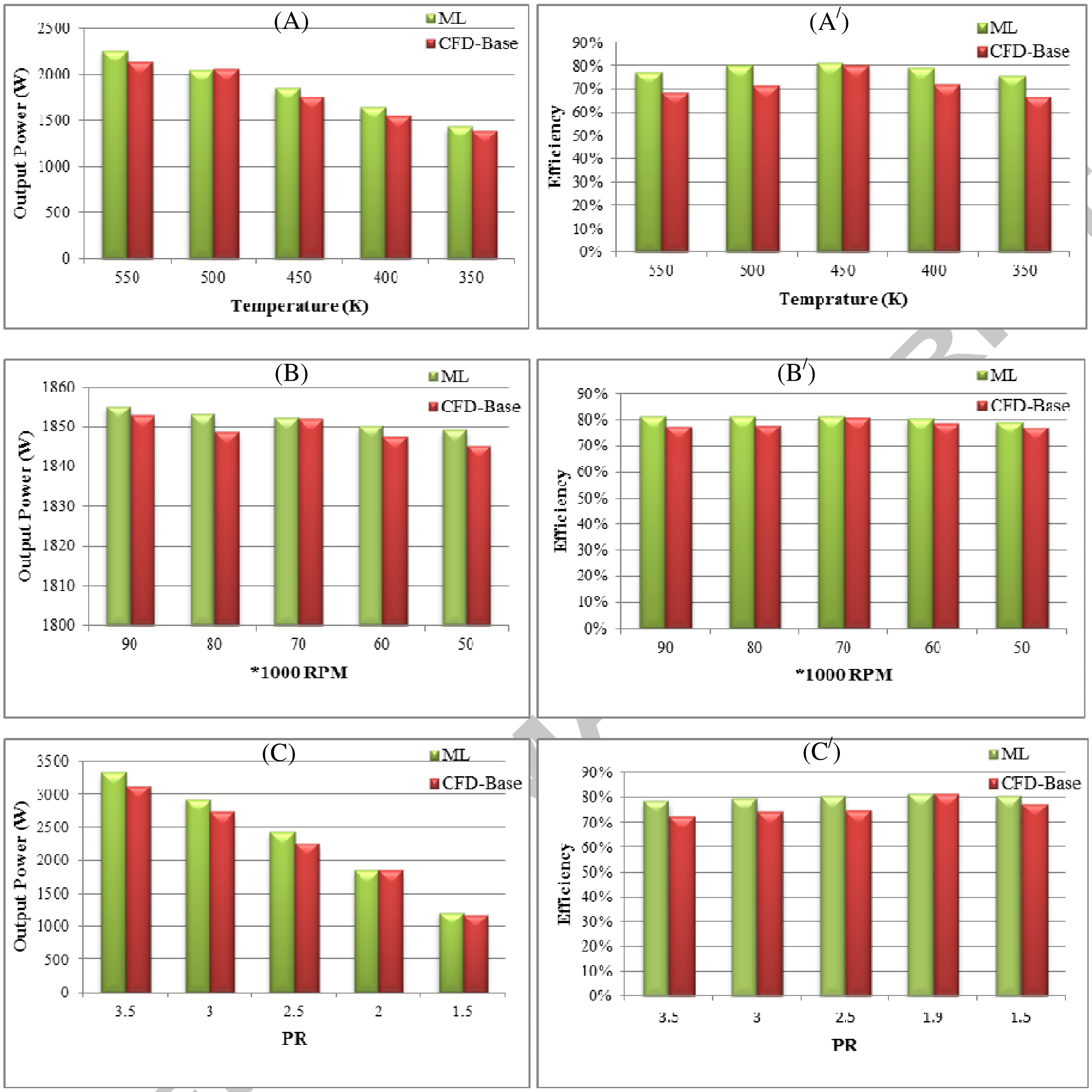

Fig. 10. Comparison between ML and CFD results; efficiency and power output at different: (A) Inlet temp, (B) Rotational speed and (C) Pressure ratio.

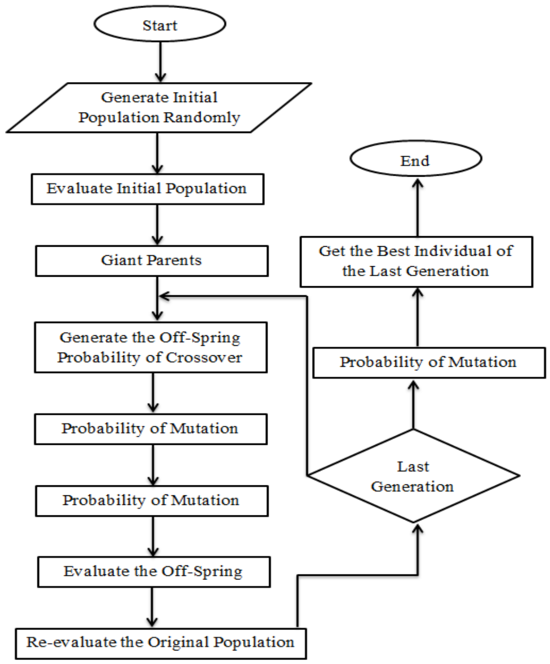

Fig. 11. Genetic algorithm flow chart.

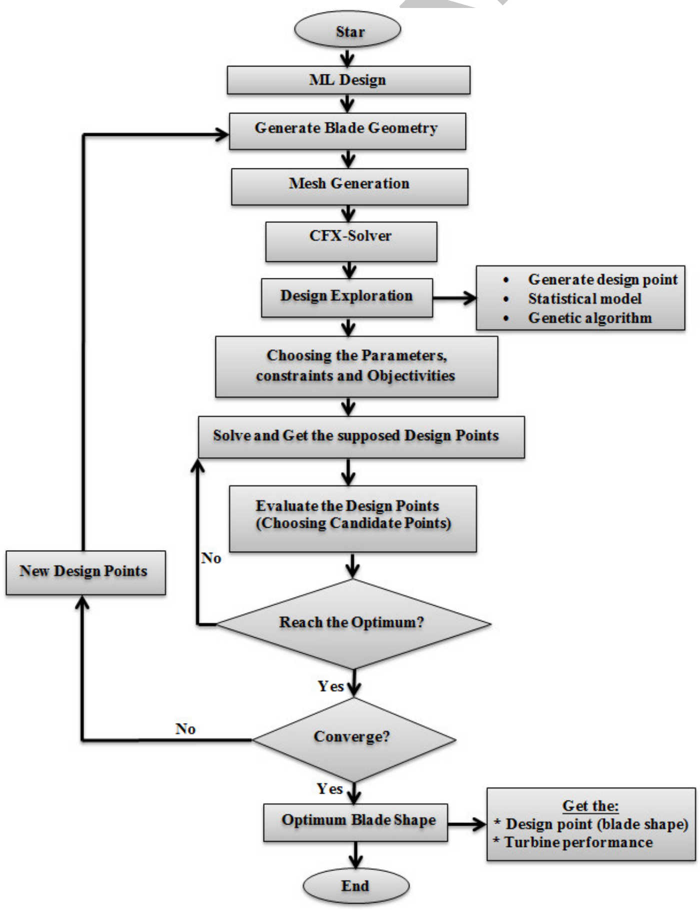

Fig. 12. The procedure followed by the three Dimensional optimization of CFD.

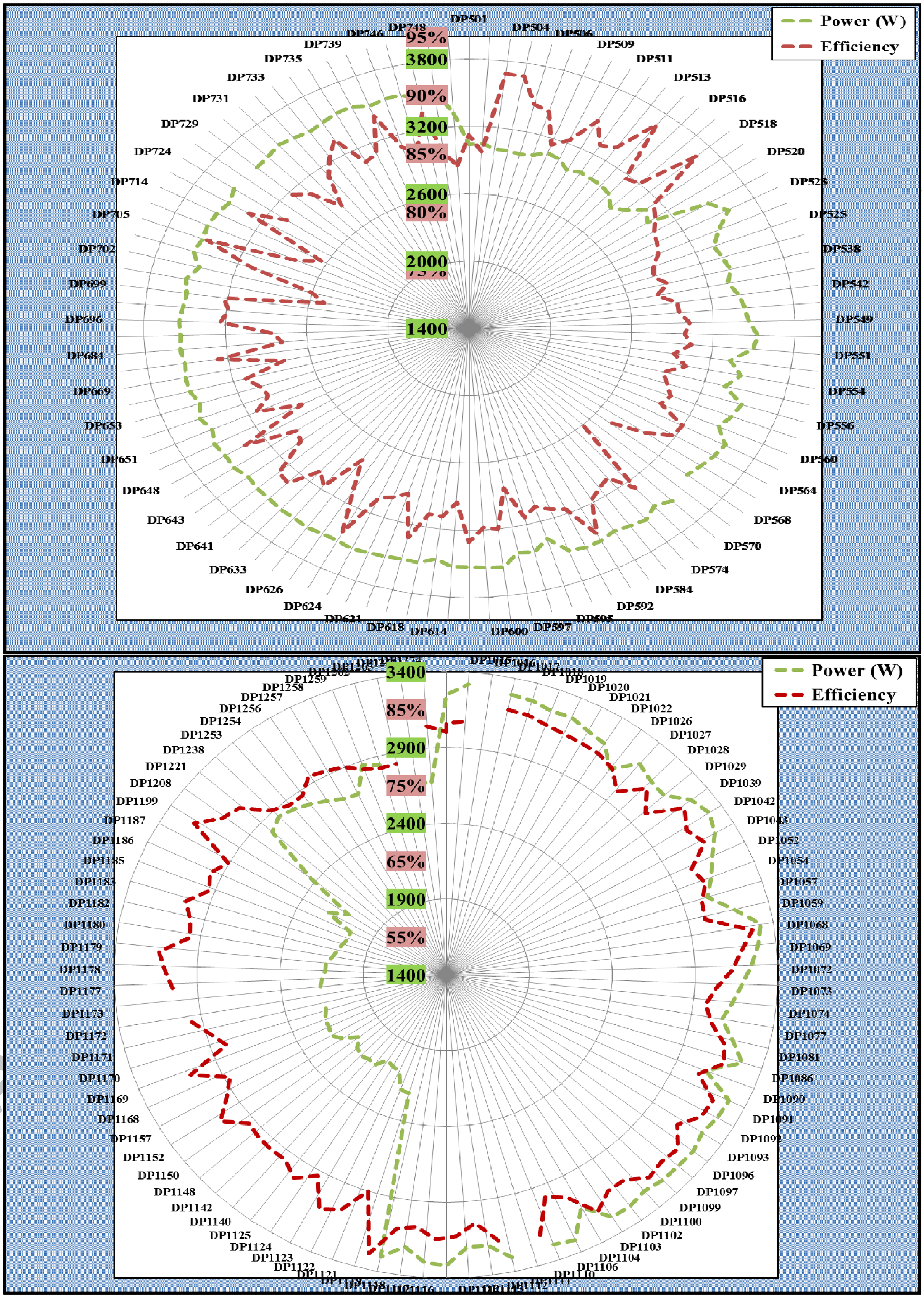

Fig. 13. Modulation of the SSRT efficiency and power output values with some of the investigated design points.

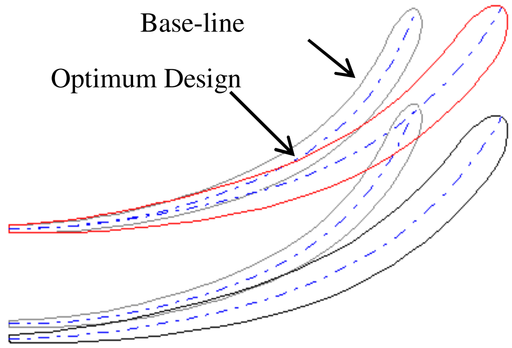

Fig. 14. Comparison between blade geometry at the base-line and optimum

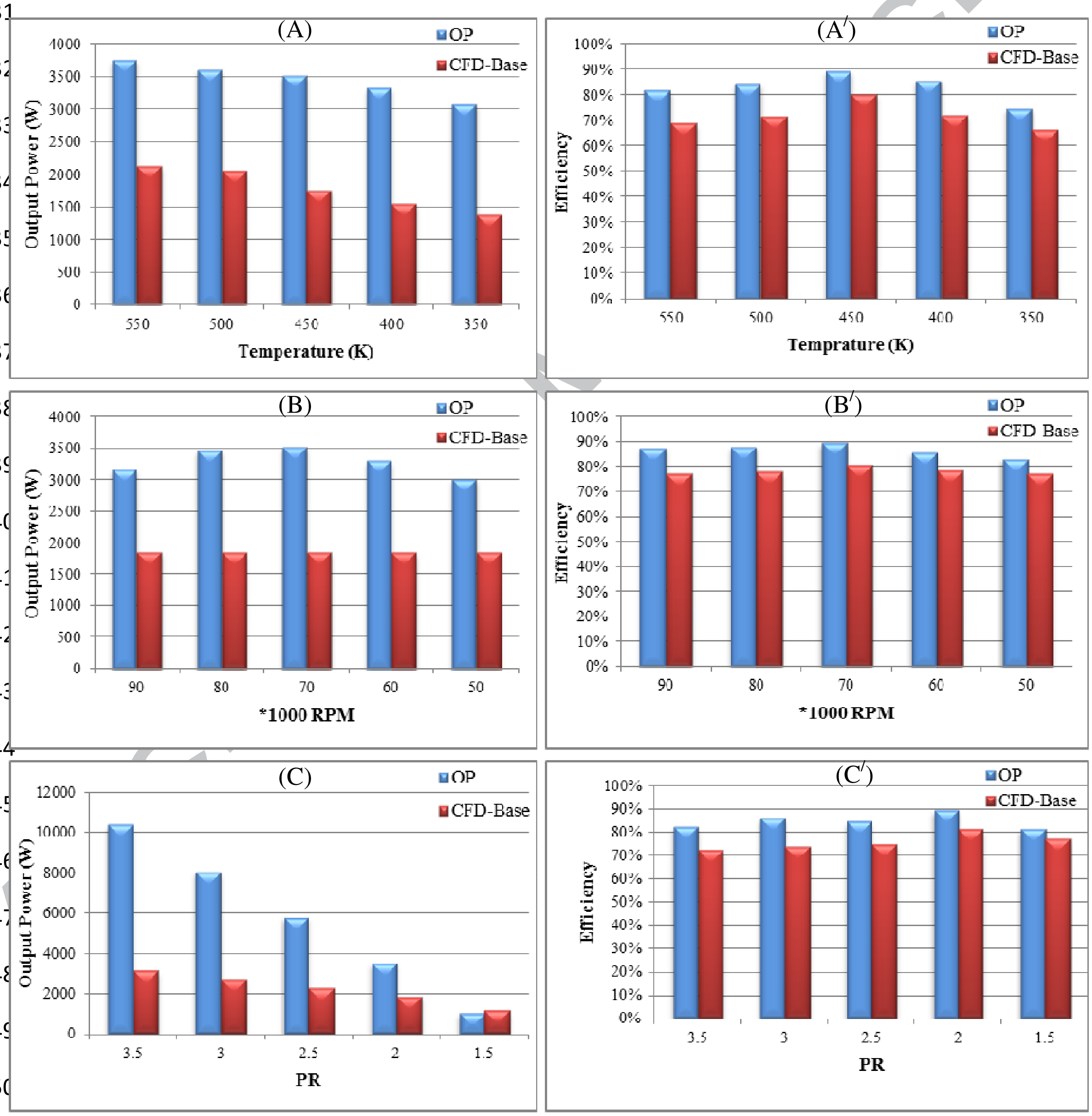

Fig. 15. Comparison between CFD and OP results; efficiency and power output at different:
(A) Inlet temp, (B) Rotational speed and (C) Pressure ratio.

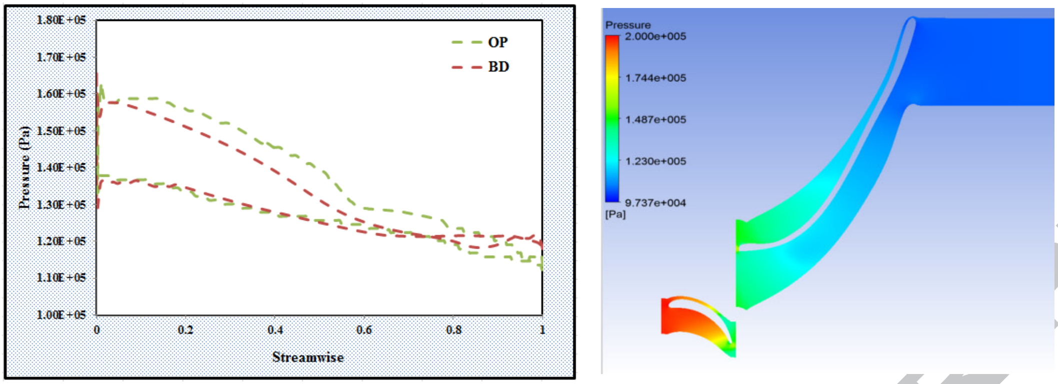

(A) (B)

Fig. 16. (A): Pressure distribution of the BL and OP for the rotor blade and (B): Contours of pressure distribution in the stator, rotor and diffuser at 50% span.

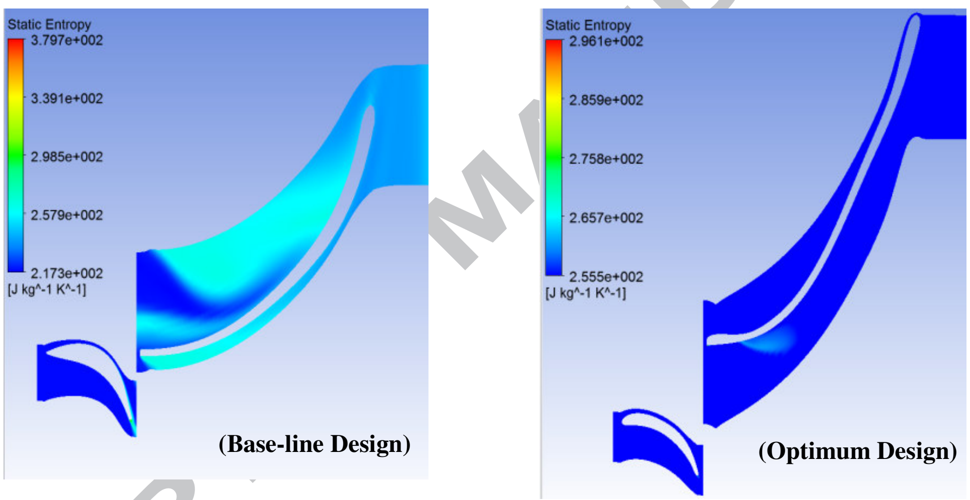

Fig. 17. Entropy generation at base-line design and optimum design.

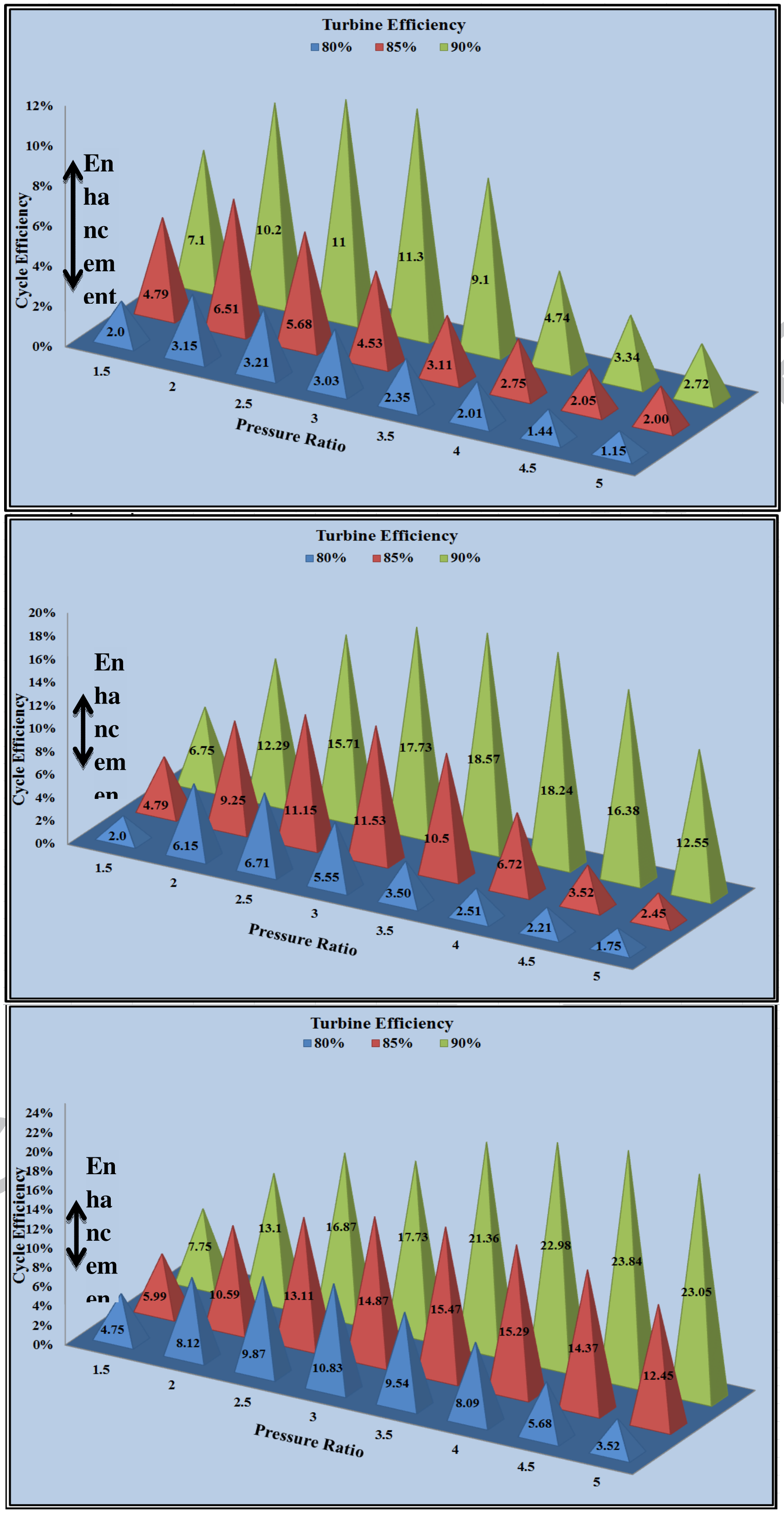

Fig. 18. The effect of pressure ratio and turbine efficiency values at inlet temperature of: (A) 450K, (B) 500K and (C) 550K on the cycle efficiency.

Table 1: Input operating conditions of integrated the radial turbine and the Brayton cycle model.

Parameter	Range/value
Loading coefficient (-)	0.8-1.4
Flow coefficient (-)	0.1-0.5
Shroud $_{Exit}$/Shroud $_{Inlet}$ (-)	0.8
Hub $_{Exit}$/Hub $_{Inlet}$ (-)	0.22
Rotational speed (rpm)	50000-90000
Inlet total temperature (K)	450 - 550
Inlet total pressure (bar)	2 -5
Mass flow Rate (kg/sec)	0.03 – 0.05
Working fluids (-)	air
Cp(J/kg K)	1005
Inlet blade velocity (m/s)	253.1
Exit blade velocity (at shroud) (m/s)	202
Inlet relative velocity(m/s)	65.8
Exit relative velocity(m/s)	206.3
Inlet absolute velocity(m/s)	250.5
Exit absolute velocity(m/s)	14.7
Rotor inlet density(kg/m^3)	1.153
Rotor inlet Mach (abs) (-)	0.7
Rotor inlet Enthalpy (J/kg)	109463
Rotor outlet Enthalpy (J/kg)	95288.8
Rotor Enthalpy at the leading edge (J/kg)	107811
Rotor Enthalpy at the trailing edge(J/kg)	87117

Table 2: The meanline characteristics of the SSRT.

Nozzle	Value	Unit	Rotor	Value
Meridional length	12.93	(mm)	Axial clearance	0.4
Blade number	28	(-)	Blade number	15
Tip width	1.7	(mm)	Axial length	11.671
Exit height		(mm)	Tip width	1.7
Inlet absolute flow angle	0	(deg.)	Inlet absolute flow angle	75
Inlet height		(mm)	Inlet height	69.06
Inlet radius	50.43	(mm)	Inlet radius	34.53
Outlet absolute flow angle	75	(deg.)	Inlet relative flow angle	-9
Outlet radius	39.71	(mm)	Outlet shroud radius	27.6
TE thickness	0.4	(mm)	Radial clearance	0.4
Throat area	95	(mm^2)	Throat area	95
Aerofoil area	33.18	(mm^2)	Aerofoil area	25.38
Camber length	17.75	(mm)	Camber length	30.975
Cord length	15.63	(mm)	Cord length	27.82
LE thickness	0.25	(mm)	LE thickness	0.25
Pitch cord Ratio	0.448	(-)	Pitch cord ratio	0.365
Solidity	2.22	(-)	Solidity	3.77
Stagger angle	34.2	(deg.)	Stagger angle	-37.1
		(deg.)	Outlet absolute flow angle	-12.5
		(deg.)	Outlet relative flow angle (hub)	-76.3
		(deg.)	Outlet relative flow angle (root mean square)	-79.3
		(deg.)	Outlet relative flow angle(shroud)	-82.1
		(mm)	Outlet hub radius	7.6
		(mm)	TE thickness	0.4

(mm)	Meridional length	22.193

815 **Table 3: The data used for validation as reported in references [46, 47].**

Parameter	Reference 46	Reference 47
Working fluid (-)	Air	Air
Mass flow rate (kg)	0.3311224	0.2313
Inlet temperature (K)	1056.483	322.2
Inlet pressure (bar)	40.02673	1.379
Pressure ratio (-)	5.7	3.255
Rotational speed (rpm)	106588	31456
Output power (kW)	37.285	15.5
Turbine efficiency (%)	87	82.7

816

817 **Table 4: The geometrical data used for validation as reported in references [46, 47].**

Parameter	Value
Rotor inlet diameter (m)	0.1504
Ratio of rotor exit tip to inlet diameters (-)	0.6275
Ratio of rotor exit hub to tip diameters (-)	0.4844
Ratio of stator exit to rotor inlet diameters (-)	1.11 1
Ratio of stator inlet vane height to rotor inlet diameter (-)	0.0726
Ratio of stator exit bane height to rotor inlet diameter (-)	0.0537
Ratio of stator inlet to stator exit diameters (-)	1.163
Number of stator vanes (-)	29
Number of rotor blades (-)	12
Specific speed (-)	0.46
Blade speed ratio (-)	0.609

818

819 **Table 5: The base-line and optimum design variable from CFD-MOGA optimization.**

Design variables	Baseline	Optimum
Stator no. of blade (-)	32	36
Stator stagger angle (deg.)	33	37.739
Stator TE Beta Angle (deg.)	69	73.70
Rotor no. of blade (-)	13	15
Rotor LE beta angle (deg.)	16.2	-46.3109
Rotor Inlet Flow Angle (deg.)	-58.3	74.03
Rotor Stagger Angle at span 0.0 (deg.)	14.4	-16.8
Rotor Stagger Angle at span 0.5(deg.)	-44.7	-37.1
Rotor Stagger Angle at span 1(deg.)	-64.5	-59.3
Rotator TE beta angle (deg.)	-18.5	-9.9457
Rotor Outlet Flow Angle (deg.)	78.9	83.36
Tip width of rotor (mm)	1.35	2.1
Rotor tip clearance (mm)	0.45	0.33

820

821

822

Highlights:

- 1D and 3D CFD analysis for compressed air radial turbine was carried out.
- Small scale radial turbine with high efficiency.
- 3D MOGA optimization for the radial turbine was achieved.
- Enhancing the performance of both the turbine and the solar powered Brayton cycle.
- Excellent agreement between the current CFD results and two experimental works from literatures.